ResearchGate

See discussions, stats, and author profiles for this publication at: https://www.researchgate.net/publication/49810874

Theoretical Study of Specific Solvent Effects on the Optical and Magnetic Properties of Copper(II) Acetylacetonate

ARTICLE *in* THE JOURNAL OF PHYSICAL CHEMISTRY A · FEBRUARY 2011

Impact Factor: 2.69 · DOI: 10.1021/jp109826p · Source: PubMed

CITATIONS
13

READS
98

6 AUTHORS, INCLUDING:

Teodorico C. Ramalho
Universidade Federal de Lavras (UFLA)
188 PUBLICATIONS **1,684** CITATIONS
SEE PROFILE

Olav Vahtras
KTH Royal Institute of Technology
130 PUBLICATIONS **4,276** CITATIONS
SEE PROFILE

Hans Agren
KTH Royal Institute of Technology
867 PUBLICATIONS **18,561** CITATIONS
SEE PROFILE

Available from: Teodorico C. Ramalho
Retrieved on: 25 January 2016

THE JOURNAL OF PHYSICAL CHEMISTRY A

ARTICLE

pubs.acs.org/JPCA

Theoretical Study of Specific Solvent Effects on the Optical and Magnetic Properties of Copper(II) Acetylacetonate

K. J. de Almeida* and T. C. Ramalho.

Departamento de Química, Universidade Federal de Lavras, CP 3037, Lavras, MG, Brasil

Z. Rinkevicius, O. Vahtras, and H. Ågren

Department of Theoretical Chemistry, Royal Institute of Technology, SE-10691 Stockholm, Sweden

A. Cesar

Departamento de Química, Universidade Federal de Minas Gerais, Avenida Antonio Carlos, 6627, CEP-31270-901, Belo Horizonte, Minas Gerais, Brasil

ABSTRACT: Specific and basicity solvent effects on the visible near-infrared electronic transitions and the electron paramagnetic resonance (EPR) parameters of the copper(II) acetylacetonate complex, $Cu(acac)_2$, have been investigated at the density functional theory level. The computed absorption transitions as well as the EPR parameters show a strong dependence on the direct coordination environment around the Cu(II) complex. High solvatocromic shifts are observed for 3d−3d transitions, with the highest effect observed for the $d_{z^2} \rightarrow d_{xy}$ transition, which is red-shifted by 6000 cm^{-1} and 9000 cm^{-1} in water and pyridine solvent models, respectively. Compared to the electronic g-tensors, the hyperfine coupling constants of the $Cu(acac)_2$ complex show a more pronounced dependence on the effect of base strength of solvent. Overall, the present methodology satisfactorily models the solvent effect on the optical and magnetic properties of the $Cu(acac)_2$ complex, and theory and experiment agree sufficiently well to warrant the use of the computed optical and EPR parameters to elucidate the coordination environment of the Cu(II) systems in basic solutions.

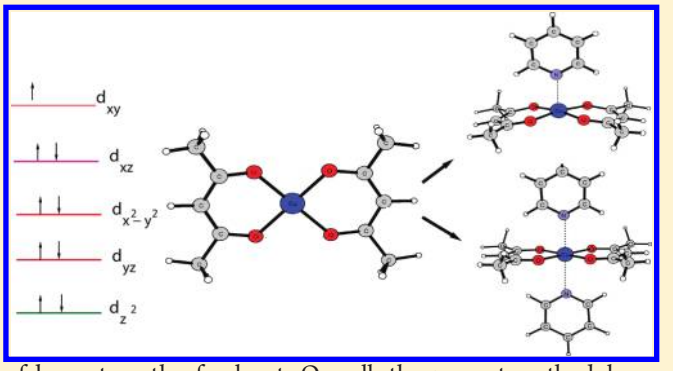

INTRODUCTION

Solvent effects on optical and magnetic properties of copper(II) compounds is a matter of considerable interest as the copper(II) ion is second only to iron in prevalence in biological systems, where most chemical processes take place in aqueous environment.[1] The interaction with solvent molecules gives rise to significant changes in the electronic and molecular structure of copper compounds, showing an important role in the determination of their properties and reactivities as well as in the structure−function relationships of copper proteins and enzymes. A common goal of ongoing investigations is to understand the dynamical behavior of molecules in various liquid environments. While experimental and theoretical studies of solvent effects on the chemical properties of organic compounds are abundant,[2−6] only little theoretical information can be found regarding transition metal complexes, and, indeed, information of solvent effects on the optical and magnetic properties of copper(II) compounds are lacking. The presence of a paramagnetic metal center is probably the limiting factor of such investigations as it requires a careful selection of the calculation methodology employed in order to ensure reliable results.

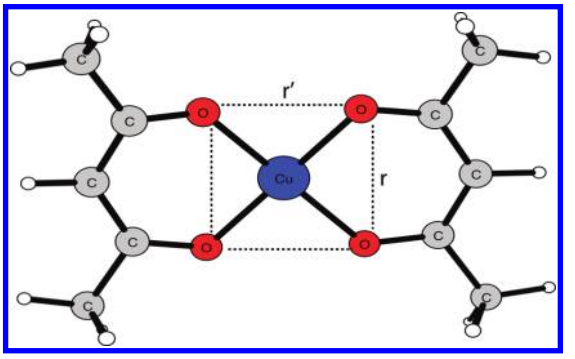

Figure 1. Molecular structure of bis(acetylacetonato)copper(II), $Cu(acac)_2$.

Significant solvatocromic effects has been experimentally observed on the optical and magnetic spectra of bis(acetylacetonato)-

Received: October 13, 2010
Revised: December 30, 2010
Published: February 4, 2011

ACS Publications © 2011 American Chemical Society

copper(II), $Cu(acac)_2$ (Figure 1).[7−10] In particular, Belford and et al.[9] studied the visible and near-infrared absorption spectra of this chelate compound in a number of different basic solvents. The behavior of absorption bands on alteration of the solvent was shown to be consistent with the crystal-field splittings. In another study carried out by Adato and Eliezer,[10] both the **g**-tensor and the anisotropy of the nuclear hyperfine interaction tensors of $Cu(acac)_2$ showed a considerable variation with respect to solvents of different basicities. The interpretation of the solvent effect in these studies has been based in terms of the influence on the spectra from the ligand-field of the closest surrounding solvent molecules. Crystal- and ligand-field theories have thus provided a standard qualitative picture of the environment effect on the optical and magnetic spectra of chelate complexes.[7] However, some questions, such as the operating mechanism of solvent molecules in Cu(II) systems and the coordination number of the Cu(II) ion in the first solvation shell of $Cu(acac)_2$ in basic solvents, remain poorly understood. While a structure with two solvent molecules coordinated at the axial position of $Cu(acac)_2$ has been claimed by Belford and et al.[9] as a classical model of the Jahn−Teller distortion, an alternative coordination with only one axial molecule in the first solvation shell was proposed by Ortolano and et al.[8] to explain the high intensities observed in the visible absorption bands of $Cu(acac)_2$ in basic solvents, such as pyridine and piperidine.

On the theoretical side, the relationship between the spectral and structural features can be successfully achieved by means of systematic calculations involving different geometries of the local coordination environment around the metal complex. However, very few theoretical investigations have yet been reported dealing with solvent effects on the optical and electron paramagnetic resonance (EPR) spectra of the copper(II) systems. Ames and Larsen have recently reported some studies by using the density functional theory (DFT) methods for the EPR parameters of the copper(II) systems.[11,12] In particular, these authors published the EPR parameters of $Cu(acac)_2$ within the tetradydrofurane and pyridine solvent models. Their results reproduce the experimentally observed trends in the parallel components of the **A**- and **g**-tensors, providing important insights into the structural basis for the empirical trends in EPR parameters of these systems.[12] Previous investigations have also been applied to investigate the optical and EPR properties of the unsolvated $Cu(acac)_2$ system.[13−17] We reported the computed visible electronic transitions as well as EPR parameters for $Cu(acac)_2$.[13,14] The DFT results showed a high dependence of the four nondegenerate 3d→3d excitation energies on the molecular distortion of the acac ligand field, while spin polarization effects on the electronic **g**- and **A**-tensors were investigated in detail for a series of square planar copper(II) complexes, including $Cu(acac)_2$ complex.[13,14] In addition, the DFT methods developed by Neese for EPR parameters have shown a good applicability for $Cu(acac)_2$ and of a class of Cu(II) compounds in the gas-phase.[15,16] Saladino and Larsen have reported the EPR parameters of the $Cu(acac)_2$ and $[Cu(ox)_2]^{2-}$ complexes at the DFT level, including the scalar relativistic and SOC effects.[17]

In this work, we report an investigation of solvent effects on the visible near-infrared absorption EPR spectra of $Cu(acac)_2$ in basic solution. The main focus of this study is to assess information about the solution environment of $Cu(acac)_2$ by means of the computed optical and EPR parameters, where a description of the first solvation shell around the chelate compound is explicitly considered. The pyridine solvent was chosen due to the experimental and computed results available for comparative purposes, so that the accuracy of the recently developed methods of our group could be assessed. The effect of solvent basicity is also taken into account in the work with the aim of evaluating the origin of these changes for the copper(II) chelate systems. For this purpose, we have selected the water due to its lower basicity, compared to that of pyridine, and also considering the importance of the hydration process of copper(II) compounds.

COMPUTATIONAL DETAILS

We have used two models for describing the first solvation shell around $Cu(acac)_2$ (acac = 2,4-pentanedione). The geometry optimizations were performed by explicitly attaching one and two solvent molecules at the axial position of the chelate complex. The *cis* and *trans* conformations of the solvent molecules in the axial position of the acac complex (see Figure 2) were considered in the calculations of the optical and EPR spectra. The description of the first solvation shell by using the supermolecule model has proved to be quite reliable for copper(II) systems since the relatively strong and specific interactions take place between $Cu(acac)_2$ and basic solvents.[18] Furthermore, the solvent effects due to long-range interactions have been evaluated by means of PCM methodology in our previous work,[19] and the obtained results showed that this effect is very small on the Cu(II) aqua and $Cu(acac)_2$ compounds (<5%) and can, therefore, be neglected in the present calculations.

Geometry optimization processes of the $Cu(acac)_2$ solvated models were carried out with no symmetry constraint at the B3LYP level in the GAMES-US program.[20] The standard Gaussian 6-31G(d) basis set was used for the copper atom,[21] while 6-311G** was employed for the oxygen and hydrogen atoms.[22] The spin-restricted open-shell density functional linear response (DFT-RL) formalism[23] was employed in the calculations of absorption transitions. The hybrid Becke3−Lee−Yang−Parr (B3LYP) exchange-correlation functional[24,25] was also used in these calculations. The present methodology has provided reliable and consistent predictions for the excitation energies for the Cu(II) aqua and acac complexes[13,19] and consequently enables us to conduct an accurate evaluation of these properties in the $Cu(acac)_2$ systems.

The electronic **g**-tensor and hyperfine coupling tensor methodologies have been described in detail in our previous paper.[18] The electronic **g**-tensors were computed using the restricted density functional approach, while a restricted-unrestricted method, evaluating the Fermi contact and spin-dipolar contributions, was used in the hyperfine coupling constant calculations. Higher order spin−orbit contributions to the hyperfine coupling tensors were computed using spin-restricted DFT-RL theory. In the evaluation of this contribution, the spin-polarization effects were neglected since they have been observed to be of minor importance in our previous studies.[14,26] All calculations of EPR parameters described above have been performed using the modified Beck3-Lee−Yang−Parr with 38% of exact exchange (B38LYP) functional reparametrized by Solomon et al.[27,28] This functional is known to reproduce the correct balance between ionic and covalent bonding character in Cu d^9 complexes, like the Cu(II) compounds here. In the electronic EPR calculations, we employed the IGLO-II basis set for the oxygen and hydrogen atoms and an extension of uncontracting the s-type functions in the IGLO-II basis,[29,30] adding two tight s-type functions. For the copper ion, the CP(PPP) basis set designed by

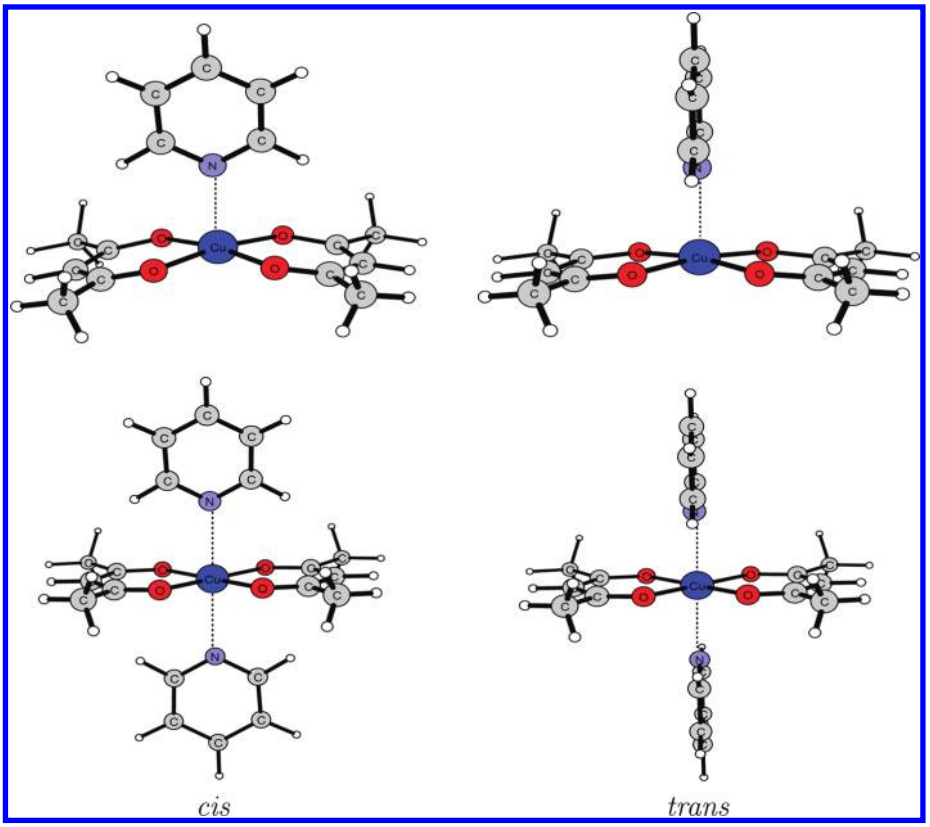

Figure 2. Optimized molecular structures of the $Cu(acac)_2$−pyridine complexes.

Table 1. Bond Lengths (in Å) and Bond Angles (in degrees) of the $Cu(acac)_2$ Systems

	$Cu(acac)_2\cdot(py)$			$Cu(acac)_2\cdot(py)_2$			$Cu(acac)_2$		
parameters[a]	*cis*	*trans*	other work[b]	*cis*	*trans*	other work[b]	C_{2h}[c]	C_{2h}[d]	other work[b]
Cu−O	1.953	1.952	1.967	1.970	1.976	1.981	1.913	1.914 ± 0.002	1.940
C−O	1.259	1.260		1.255	1.258		1.272	1.273 ± 0.002	
C−CH	1.401	1.400		1.404	1.401		1.402	1.402 ± 0.003	
$C-CH_3$	1.508	1.508		1.510	1.510		1.516	1.512 ± 0.004	
Cu−N(Solv)	2.319	2.305	2.397	2.510	2.449	2.579			
r	2.746	2.732		2.801	2.781				
r′	2.756	2.772		2.772	2.809				
∠Cu−O−C	128.3	127.7		128.4	127.1		125.1	124.8 ± 0.4	
$\angle O-C-CH_3$	115.4	115.3		115.5	115.4		115.5	115.7 ± 1.0	
∠O−C−CH	125.2	125.4		125.3	125.7		124.9	124.4 ± 0.5	
∠O−Cu−O	89.8	90.5		89.4	90.6		92.4	92.3 ± 0.9	
∠O′−Cu−O′	89.4	88.8		90.6	89.4		87.6		

[a] *r* and *r*′ parameters correspond to oxygen−oxygen distances as shown in Figure 1. [b] The B3LYP optimized parameters of Ames and Larsen from ref 12. [c] Our previous B3LYP results from ref 13. [d] Experimental results of neutron diffraction in gas phase from ref 37.

Neese[31] for accurate calculations of the hyperfine coupling in transition metal compounds was used. Our choice of basis set is not compatible with the standard routines for AMFI spin−orbit operator matrix elements implemented in DALTON 2.0, and in order to overcome this limitation, we employed the code provided by Schimmelpfennig,[32] which is capable of evaluating AMFI SO matrix elements for arbitrary basis sets. All calculations for the absorption transitions and EPR spin Hamiltonian parameters were carried using the DALTON 2.0 quantum chemistry package.[33]

RESULTS AND DISCUSSION

Complex Geometries. The optimized molecular structures of the $Cu(acac)_2$−pyridine complexes are shown in Figure 2. The computed and experimental bond lengths and bond angles of the $Cu(acac)_2$ systems are collected in Table 1. The structures of $Cu(acac)_2$−pyridine systems are characterized by strongly coordinated atoms of acac ligands at equatorial position, whereas one or two solvent molecules are weakly coordinated at axial position, leading to the distorted square pyramidal and octahe-

Table 2. Experimental and Calculated Excitation Energies (in cm^{-1}) and Oscillator Strengths in the $Cu(acac)_2$−Pyridine Complexes

	$Cu(acac)_2\cdot(py)$				$Cu(acac)_2\cdot(py)_2$						
	cis		*trans*		*cis*		*trans*		exp.		
transition	E (cm^{-1})	f^a	E (cm^{-1})	f^a	E (cm^{-1})	f^a	E (cm^{-1})	f^a	sol.[b]	sol.[c]	$f^{c,b}$
I	10535	0.0	10481	0.0	8100	0.0	6718	0.0		10200	3.6
II	13241	3.0	13169	5.0	12265	0.0	11803	0.0	12100	12700	4.7
III	15031	10.6	15216	7.1	13546	0.0	13946	0.0	14800	14900	7.7
IV	15534	0.0	15867	0.0	14713	0.0	14861	0.0	15100	15200	2.2

[a] Oscillator strength × 10^{-4}. [b] Experimental data of $Cu(acac)_2$ in the pyridine solution from ref 9. [c] Experimental data of $Cu(acac)_2$ in the pyridine solution from ref 8.

dral atomic arrangements, respectively. As shown in Table 1, our previous results for the bond lengths and bond angles of the gas-phase $Cu(acac)_2$ complex reproduce quite well the experimental gas-phase data of this complex, with the maximum errors of 0.004 Å and 0.5 degree for bond lengths and bond angles, respectively. The B3LYP result reported by Ames and Larsen indicate a larger Cu−O bond length for $Cu(acac)_2$, with a deviation of 0.03 Å.[12] A comparison between the solvated and nonsolvated structures gives us some important information about the solvent effect on the geometrical parameters of this complex. Overall, the coordination of the solvent molecules at the axial position of $Cu(acac)_2$ give rises to significant changes in its Cu−O bond lengths and O−Cu−O bond angles, whereas the other geometrical parameters of acac ligands remain nearly unchanged. The results show that a progressive increase of 0.04 Å and 0.06 Å in the Cu−O bond lengths is observed in the $Cu(acac)_2\cdot(py)$ and $Cu(acac)_2\cdot(py)_2$ systems, respectively. A smoother trend was, however, verified by Ames and Larsen, in which larger absolute values (0.06 Å in average) are computed for the Cu−O and Cu−N bond lengths relative to the present results. These geometrical differences can be taken as an indication of the use of different atomic basis sets. The increasing behavior of Cu−O bond lengths with the axial coordination has been experimentally observed in crystal structure analysis of the anhydrous and hydrates copper(II) hexafluoroacetylacetonate complexes as well as in the aqueous hydrated copper(II) ion.[12,18,34]

The Cu atom in *cis* and *trans* mono−pyridine complexes are displaced 0.2 Å and 0.15 Å, respectively, out of the plane of the four acac O atoms toward the coordinated pyridine molecule. Comparing the energetics of solvent complex models, the *trans* conformations are more stable than *cis* geometries in a range between 2 and 4 cal mol^{-1}. By analyzing the B3LYP total atomic spin densities, which can be taken as a measure of covalent delocalization for the single unpaired 3d-electron over the $Cu(acac)_2$ complex, a range of values varying from 0.28 electrons (Cu spin density 0.70e) to 0.25 electrons (Cu spin density 0.73e) were computed to the $Cu(acac)_2$−pyridine complexes. These quantities are equally distributed from the copper(II) ion onto the oxygen atoms of the acac ligands in the solvated Cu(acac) complexes. The total atomic spin density on the N atoms of solvent molecules is not higher than 0.001e in all the complexes investigated. Thus we can conclude that the covalent character of chemical bonds of $Cu(acac)_2$ are restricted to the equatorial bonds, whereas weak electrostatic interactions of solvent molecules should take place at the axial positions of this complex.

The Visible Absorption Transitions. The computed and experimental excitation energies and oscillator strengths of the $Cu(acac)_2$−pyridine complexes are listed in Table 2. Four nondegenerate electronic transitions were computed irrespective of whether $Cu(acac)_2\cdot(py)$ or $Cu(acac)_2\cdot(py)_2$ complexes are considered. This is an important result since there still remains in the literature a divergent view about the number of the electronic transitions in the visible absorption spectrum of $Cu(acac)_2$, which is not well resolved in isotropic media. Whereas Belford et al.[9] used a model of three bands to interpret the absorption transitions in different solutions, Ortolano and Funck[8] give their interpretation in terms of a model of four bands. The DFT results of monopyridine $Cu(acac)_2$ complexes show a better agreement with the experimental results of Ortolano and Funck, with an average deviation of 335 cm^{-1} and the largest errors of 541 cm^{-1} being observed for transition II of the *cis* conformation. The calculated absorption positions in the $Cu(acac)_2\cdot(py)_2$ complexes are localized at lower energies than those in the $Cu(acac)_2\cdot(py)$ complexes. This behavior becomes more pronounced for the transition I, which shows an average shift of about 3000 cm^{-1} when two $Cu(acac)_2$−pyridine models are compared.

With regard to absorption intensities, the oscillator strengths computed show values equal to zero for all electronic transitions of the $Cu(acac)_2\cdot(py)_2$ complexes (D_{2h} symmetry), whereas the oscillator strengths of two transitions in the noncentrosymetric $Cu(acac)_2\cdot(py)$ complexes (C_{2v} symmetry) are computed between 3.0×10^{-4} and 11.0×10^{-4}. These results arise from the fact that the 3d→3d transitions in the copper(II) compounds are forbidden by Laporte selection rule ($\Delta l = \pm 1$) and, consequently the computed electronic oscillator strengths are all equal to zero in the D_{2h} and C_{2h} symmetries as well as in the two transitions of the C_{2v} ($Cu(acac)_2$−(py)) structures since vibronic coupling effects are not included in the present calculations. The B3LYP values of the *trans* conformation agree very well with the experimental of results, indicating, therefore, that the electronic contribution should be the dominating part of the experimental intensities observed for these transitions. The visible near-infrared excitation energies in the acac pyridine complexes are assigned to be 3d→3d-based transitions localized mainly on the copper(II) ion. The optimized molecular orbitals of the *trans*-$Cu(acac)_2\cdot(py)$ complex are displayed in Figure 3. The same ordering of 3d-orbitals is obtained for both $Cu(acac)_2$−pyridine models. The ground-state d_{xy}, which is well established experimentally for $Cu(acac)_2$ and the related acac complex,[35] was correctly accounted for by B3LYP calculations of these complexes. The $d_{xy} > d_{z^2} > d_{yz} > d_{xz} > d_{x^2-y^2}$ order is in full agreement with the experimental assignment of Ortolano and Funck for the absorption spectrum of $Cu(acac)_2$ in pyridine solution.[8]

dx.doi.org/10.1021/jp109826p |J. Phys. Chem. A 2011, 115, 1331–1339

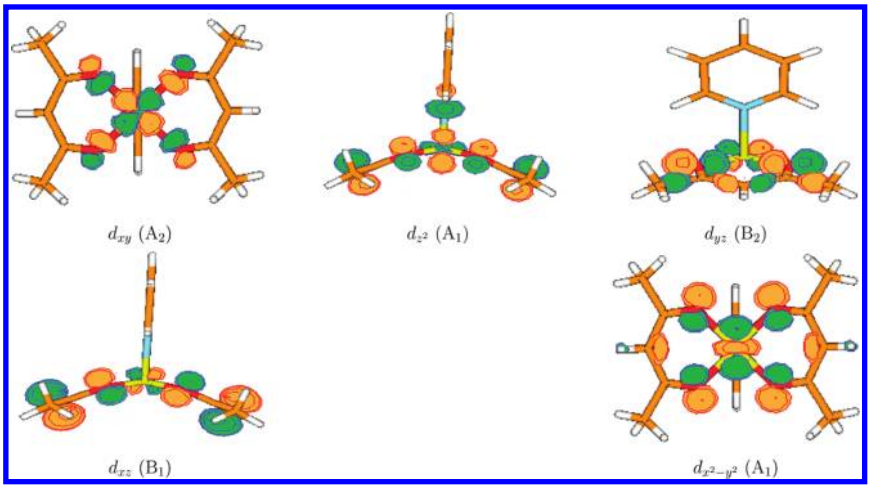

Figure 3. The B3LYP molecular orbitals involved in 3d−3d electronic transitions of the monofold-coordinated Cu(acac)$_2$−pyridine complex. The symmetry of the *d*-orbitals within the C_{2v} point group is shown in parentheses.

Table 3. Experimental and Calculated g-Tensors (in ppt) in the Cu(acac)$_2$−Pyridine Complexes

	Cu(acac)$_2$·(py)				Cu(acac)$_2$·(py)$_2$				
	cis	*trans*	other work[a]		*cis*	*trans*	other work[a]		
g tensor	B38LYP	B38LYP	BP86	B3LYP	B38LYP	B38LYP	BP86	B3LYP	exp.[b]
g_{xx}	2.0839	2.0835			2.1176	2.1132			2.0859
g_{yy}	2.0848	2.0828			2.1083	2.1056			2.0859
g_{zz}	2.2889	2.2824	2.127	2.190	2.3211	2.3245	2.135	2.201	2.2736
g_o	2.1525	2.1496			2.1823	2.1845			2.1485

[a] The calculated absolute $\mathbf{g}_{\|}$ tensors of Cu(acac)$_2$−pyridine complexes from ref 12. [b] Experimental results of Cu(acac)$_2$ in pyridine solution (in cm^{-1}) from ref 10.

Table 4. Hyperfine Coupling Constants of ^{63}Cu Dication (in MHz) in the Cu(acac)$_2$−Pyridine Complexes

compound	model	functional	A_{xx}	A_{yy}	A_{zz}	A_{iso}	A_{FC}	A_{xx}^{dip}	A_{yy}^{dip}	A_{zz}^{dip}	A_{xx}^{SO}	A_{yy}^{SO}	A_{zz}^{SO}
Cu(acac)$_2$·(py)	*cis*	B38LYP	73	76	−550	−134	−330	301	301	−603	105	111	373
	trans	B38LYP	69	74	−557	−138	−332	301	301	−602	103	111	366
other work[a]	square pyramidal	BP86			475								
		B3LYP			554								
Cu(acac)$_2$·(py)$_2$	*cis*	B38LYP	100	104	−525	−107	−318	305	305	−611	115	122	393
	trans	B38LYP	96	99	−536	−114	−321	305	305	−610	112	121	385
other work[a]	octahedral	BP86			469								
		B3LYP			542								
experiment[b]			8.84	8.84	489	169							

[a] The calculated absolute $\mathbf{A}_{\|}$ tensors of Cu(acac)$_2$−pyridine complexes from ref 12. [b] Experimental results of Cu(acac)$_2$ in pyridine solution (in cm^{-1}) from ref 1010.

Overall, the results discussed above show that each model of the solvated complex gives rise to a particular spectral pattern of the absorption spectrum, where both positions and intensities of the visible near-infrared electronic transitions can be used to characterize the coordination environment of the Cu(acac)$_2$ complex in solution. The results of the electronic excitations indicate the square pyramidal Cu(acac)$_2$−pyridine system as the best model to describe the experimental visible absorption spectrum of Cu(acac)$_2$ in pyridine.

The Electronic g- and A-Tensors. The computed and experimental EPR parameters of the Cu(acac)$_2$−pyridine complexes are tabulated in Table 3 and Table 4, respectively. As becomes evident from the presented results in Table 3, the calculated electronic **g**-tensors of all complexes have the same ordering of individual components, i.e, $g_{zz} > g_{yy} \approx g_{xx}$, showing a complete agreement with the experimental data.[10] A systematic shift to lower values is observed for all components of **g**-tensors going from the Cu(acac)$_2$·(py)$_2$ to the Cu(acac)$_2$·(py) models. This trend can be correlated with the increased Cu−O bond lengths of the optimized complexes as the successive coordination of one and two solvent molecules takes place at the axial position of Cu(acac)$_2$. This feature has already been discussed by Ames and Larsen for some tetragonal Cu(II) model complexes with oxygen

ligands.[12] That is, the shorter Cu−O bond lengths of unsolvated $Cu(acac)_2$, as compared to those of $Cu(acac)_2$−pyridine system, are related to the greater sharing of electron density between the copper metal center and the acac ligands, leading to a delocalization of electron density on the Cu(II) ion, with a concomitant decrease in the **g**-tensors of the former systems. It is worth noting that this tendency is observed in the experimental data in the Peisach−Bumberg truth tables.[36]

The individual **g**-tensor values of *cis* and *trans* structures are slightly different from each other, whereas a larger deviation is observed in the isotropic values of these conformations. A more pronounced difference is observed for all components of g-tensors of mono- and dicoordinated $Cu(acac)_2$−pyridine complexes. The largest component, $\mathbf{g}_{zz}$, has a dominantly large local spin−orbit contribution and is shifted 0.04 ppt from $Cu(acac)_2\cdot(py)$ to $Cu(acac)_2\cdot(py)_2$ systems, showing strong dependence with respect to the number of solvent molecules coordinated at the axial position of $Cu(acac)_2$. The $\mathbf{g}_{xx}$ and $\mathbf{g}_{yy}$ components of the **g**-tensor undergo a slightly lower shift of 0.03 ppt in this molecular complex sequence. The best agreement with experimental results is obtained for the calculated values of the *trans*-$Cu(acac)_2\cdot(py)$ complex. The major discrepancy is observed for the $\mathbf{g}_{zz}$ value of this complex, which is overestimated by 0.01 ppt relative to the experimental value. Previous DFT calculations underestimate the $\mathbf{g}_{\|}$ tensors of $Cu(acac)_2$−pyridine complexes, in about 0.15 ppt, showing only a slight difference between $\mathbf{g}_{\|}$ values of square pyramidal and octahedral models, independently of the BP86 and B3LYP exchange-correlation functionals employed. This might be due to the fact that the conventional exchange-correlation functionals still remain severely handicapped in their ability to describe EPR parameters of transition metal complexes. It is important to note that for the previous calculations cited, the unrestricted Kohn−Sham (UKS) formalism was used, whereas the present results of the **g**-tensor were obtained using the restricted Kohn−Sham (RKS) approach. A comparison with experimental data available shows that the present B38LYP/RKS calculations are able to describe very well the individual components as well as the isotropic values of the **g**-tensors of the $Cu(acac)_2\cdot(py)$ and $Cu(acac)_2\cdot(py)_2$ complexes, clearly favoring the 5-fold-coordinated system for modeling the absorption spectra of $Cu(acac)_2$ in pyridine solution.

The computed Cu(II) hyperfine coupling tensor results of the $Cu(acac)_2$−pyridine complexes in Table 4 show a unique ordering of principal values as that found in the electronic g-tensor results, i.e., $|\mathbf{A}_{zz}| > |\mathbf{A}_{yy}| > |\mathbf{A}_{xx}|$. An inspection of Table 4 reveals a small variation, lower than 10 MHz, for the individual and isotropic components of the *cis* and *trans* conformations. Comparing $Cu(acac)_2\cdot(py)$ and $Cu(acac)_2\cdot(py)_2$ complex models, however, the differences between the computed hyperfine coupling values become more pronounced around 25 MHz. A progressive increase of the absolute values is observed in the $\mathbf{A}_{xx}$ and $\mathbf{A}_{yy}$ values with the subsequent axial coordination of one and two pyridine molecules in $Cu(acac)_2$, whereas a decrease of the $\mathbf{A}_{zz}$ and $\mathbf{A}_{iso}$ components is found in this sequence of complexes. The comparison between absolute values is valid since in the experimental EPR measurements, one can only determine the absolute values of the EPR hyperfine parameters. It is worth noting that the absolute $A_{\|}$ values of the $Cu(acac)_2$ system, reported by Ames and Larsen, show the same decreasing behavior as solvent models are considered for the Cu(II) model with oxygen ligands.[12] It is interesting to note that the B3LYP results are very close to the present results of **A**-tensors, whereas a higher deviation is observed with respect to the BP86 results. These results indicate once again the high dependence of **A**-tensors in terms of the exchange-correlation functional employed.

The contributions of the various components of the copper hyperfine coupling tensors should be understood so that their impact on calculation results for the hyperfine coupling becomes clear. In conventional hyperfine coupling calculations, only the Fermi contact and spin-dipolar contributions are evaluated. This procedure is well suited for organic radicals, but fails severely for transition metal compounds, where the spin−orbit contribution becomes quite important. For $Cu(acac)_2$−pyridine complexes, the Fermi contact term (A_{FC}) varies from 330 MHz $Cu(acac)_2\cdot(py)$ to 320 MHz in the $Cu(acac)_2\cdot(py)_2$ complexes. In the spin dipolar contributions ($\mathbf{A}_{ii}^{dip}$, $i = x, y, z$), the $\mathbf{A}^{dip}$ components follow a $|\mathbf{A}_{zz}| > |\mathbf{A}_{yy}| \approx |\mathbf{A}_{xx}|$ pattern (where $\mathbf{A}_{zz}$ is negative) in both models of the pyridine acac complexes. The ordering and sign patterns of the spin-dipolar contributions are in agreement with the pattern observed in the total hyperfine coupling tensors. The following ordering of $|\mathbf{A}_{zz}| > |\mathbf{A}_{xx}| > |\mathbf{A}_{yy}|$ is observed for the spin−orbit contribution ($\mathbf{A}_{ii}^{SO}$ in Table 4, $i = x, y, z$), which indeed plays a crucial role for both principal values of **A**(Cu) and $\mathbf{A}_{iso}$(Cu). For the principal values, the spin−orbit contribution (being opposite in sign to the Fermi contact contribution and of similar magnitude) effectively counteracts the Fermi contact contribution in the total hyperfine coupling tensor. Dramatic effects of the inclusion of spin−orbit coupling are observed for the isotropic hyperfine coupling constants, thus indicating that the spin−orbit interaction is of major importance for a reliable description of the hyperfine coupling constants of the $Cu(acac)_2$−pyridine complexes.

As shown in Table 4, a comparison with experimental results shows that the absolute values of the isotropic Cu(II) hyperfine coupling tensors appear to be the best EPR parameter to be exploited to judge the coordination environment of the first solvation shell around $Cu(acac)_2$ in pyridine solution. The computed values of the monopyridine $Cu(acac)_2\cdot(py)$ system show a better qualitative agreement with the experimental data available. An average deviation of 35 MHz from the experimental data is observed, likely caused by the absence of vibrational environmental effects, which would probably improve the computational results of these systems. Finally, the solvent effects on the EPR parameters of $Cu(acac)_2$ might be explained as a consequence of the localization of electron density on Cu(II), mainly caused by the increase of the Cu−O bond lengths of $Cu(acac)_2$ due to the subsequent axial coordination of solvent molecules in $Cu(acac)_2$. As a consequence from this fact, relatively higher **g**-tensors and smaller absolute values of $\mathbf{A}_{iso}$ are expected for the $Cu(acac)_2$−pyridine complexes relative to those observed in the gas-phase $Cu(acac)_2$ system. A comparison between experimental and computed $\mathbf{A}_{iso}$ values of $Cu(acac)_2\cdot(py)$ complexes gives support to our conclusions obtained from calculations of the electronic transitions and *g*-tensors, which point out the mono−pyridine complex as the most suitable model for describing the optical and magnetic properties of $Cu(acac)_2$ in pyridine solution. In summary, the good agreement between calculated and experimental results of the visible near-infrared transitions and EPR parameters shows that the present methodology is indeed consistent for modeling the solvent effects on the optical and magnetic properties of the $Cu(acac)_2$ complex in pyridine solution.

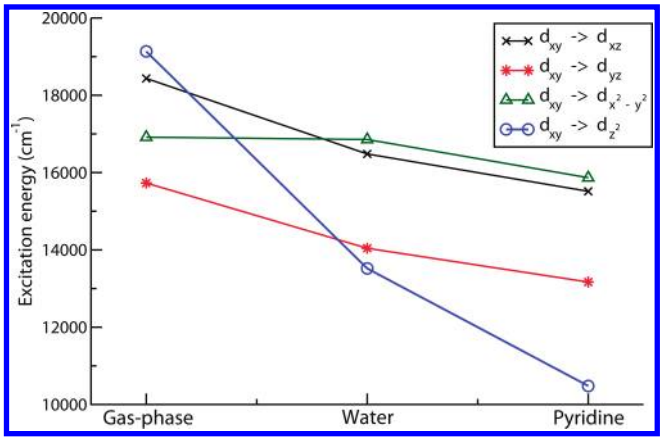

Figure 4. Solvatocromic shifts of the 3d−3d excitation energies of $Cu(acac)_2$ in different phase models.

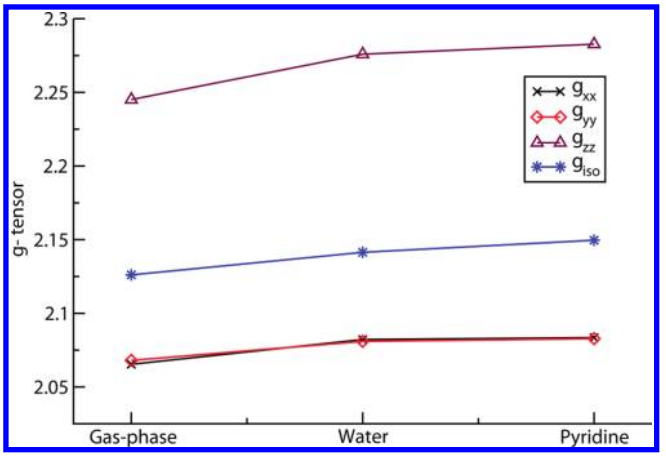

Figure 5. Solvatocromic shifts of the electronic **g**-tensors of $Cu(acac)_2$ in different phase models.

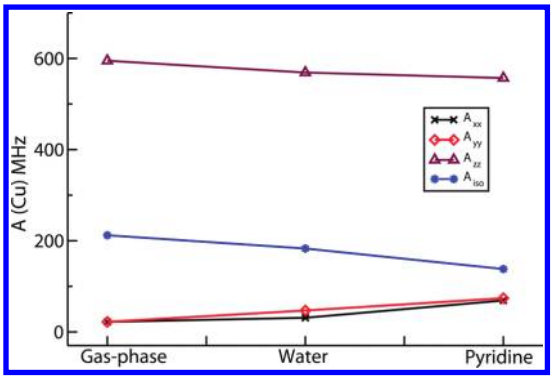

Figure 6. Solvatocromic shifts of the absolute Cu(II) hyperfine coupling constants (**A**) of $Cu(acac)_2$ in different phase models.

Solvent Basicity Effects. In order to evaluated the basicity solvent effects, we have selected the square pyramidal conformation of solvated complexes due to its better performance to describe the experimental data of optical and EPR spectra of $Cu(acac)_2$ in pyridine. The B3LYP results for the 3d−3d electronic transitions of $Cu(acac)_2$ in the gas-phase, water and pyridine solvent models are displayed in Figure 4. Overall, the results show that the coordination of solvent molecules at the axial position of $Cu(acac)_2$ acts to gradually shift each 3d→3d electronic transition to lower energies as compared to those in the gas phase, where no solvent molecules are coordinated at the axial position. It is worth noting that the extension of the computed shifts correlates with the basicity of the considered solvents, showing lower redshift values in water than in the pyridine solvent model. This feature might be ascribed to the more efficient interaction of the nonligand $p_z(N)$ orbital of pyridine, as compared to $p_z(O)$ orbital of water, with the paired electrons in the d_{z^2} orbital of $Cu(acac)_2$ (See Figure 3). Another interesting result is that distinct solvatocromic shifts are found for four 3d→3d electronic transitions. The ordering of the 3d orbitals changes from $d_{xy} < d_{xz} < d_{x^2-y^2} < d_{yz} < d_{z^2}$ in the gas-phase to $d_{xy} < d_{z^2} < d_{xz} < d_{yz} < d_{x^2-y^2}$ in the solvated model structures of water and pyridine $Cu(acac)_2$ complexes, for which the same pattern of 3d orbital order is found. The $d_{x^2-y^2} \rightarrow d_{xy}$ transition undergoes the smallest solvatocromic shift, remaining at about 16500 cm^{-1}, in agreement with the experimental referred band of $Cu(acac)_2$ in different solutions.[9,10] On the other hand, the more pronounced solvatocromic effect is observed for the $d_{z^2} \rightarrow d_{xy}$ transition, which is red-shifted about 6000 cm^{-1} and 9000 cm^{-1} in the water and pyridine complex models, respectively. The latter result is in very good agreement with the experimental value in pyridine (8600 cm^{-1}) reported by Ortolano and Funck.[8] This result may be caused by the direct interactions of the p_z orbitals of the donor oxygen and nitrogen atoms of solvents with the $d_{z^2}(Cu)$ orbitals as shown in Figure 3. Finally, we can see from this figure that there is no direct interaction of the d_{xz} and d_{yz} orbitals with the solvent orbitals and the analogous solvatocromic shifts computed for the $d_{xz} \rightarrow d_{xy}$ and $d_{yz} \rightarrow d_{xy}$ transitions can be taken as indication of this fact. It is worth noting that all above-discussed results are in complete agreement with the experimental $Cu(acac)_2$ spectra in solution.

The electronic **g**-tensors and absolute values of **A**-tensors of $Cu(acac)_2$ in the gas-phase and aqua and pyridine solvent models are shown in Figures 5 and 6, respectively. Regarding the change from gas-phase to solvent models, these figures indicate a similar and smooth increase of the electronic **g**-tensors as well as in the $\mathbf{A}_{xx}$ and $\mathbf{A}_{yy}$, whereas a pronounced decrease is verified in $\mathbf{A}_{zz}$ and $\mathbf{A}_{iso}$. These trends are correlated with those observed in EPR results as one and two pyridines coordinated at the axial position of $Cu(acac)_2$. The calculated Cu−O bond lengths of the square pyramidal aqua and pyridine $Cu(acac)_2$ solvent models are 1.932 Å and 1.953 Å, respectively. The Cu−O(water) bond lengths are computed to be 2.326 Å, while a value of 2.305 Å is found for the Cu−N(pyridine) distance. These results show an increase of the Cu−O bond lengths with the increase of the basicity solvent. Thus the observed trends in EPR parameters due to the solvent effects are related to the localization of electron density on the transition metal center. That is, the longer the Cu−O bond distance, the more localized electron density is found on the Cu(II) center, leading to a increase in the **g**-tensors, $\mathbf{A}_{xx}$ and $\mathbf{A}_{yy}$ as well as a concomitant decrease in the absolute values of $\mathbf{A}_{zz}$ and $\mathbf{A}_{iso}$ tensors. Another point relative to the solvent trends in the EPR and optical parameters of $Cu(acac)_2$ is due to differing copper deviations from the complex plane for the different solvents. The half-step (θ) parameter, which corresponds to the distance of the copper(II) ion from the acetylacetonate ligand plane, gives us some insights in this respect. The B3LYP prediction for θ in the C_{2h} structure of $Cu(acac)_2$ is 0.27 Å, while an experimental value of 0.41 ± 0.07 Å has been determined for $Cu(acac)_2$ in the gas phase. The average values in monopyridine and monowater acac complexes decrease to 0.18 Å and 0.13 Å,

dx.doi.org/10.1021/jp109826p |J. Phys. Chem. A 2011, 115, 1331–1339

respectively, whereas a value equal to zero is found for all complexes with two solvent molecules coordinated at axial position of $Cu(acac)_2$. These results suggest a correlation between the solvent trends in the EPR and optical spectra of acac complexes and the bonding θ parameter.

By careful inspection of the individual results, we can see that the hyperfine constants show a more pronounced dependence on the base strength compared to the electronic **g**-tensor. While only a slight increase of all **g**-tensor components is observed with the change of environment, a more significant variation in the nuclear hyperfine interaction constants is found for the isotropic and major component of **A**-tensors as going from the gas phase to the solvated structures. The computed values of $\mathbf{A}_{iso}$ vary from −212 MHz in $Cu(acac)_2$ to −183 MHz in $Cu(acac)_2$−water and −138 MHz in the $Cu(acac)_2$−pyridine model. The results arise mainly from the fact that the magnitude of the hyperfine splitting depends on the magnetic moment of the nucleus and how tightly the unpaired electrons are bound to it. In the basic solvents, such as water and pyridine, the O and N atoms act as the donor atoms in most adducts. It is expected, therefore, that the interactions between the donor solvent and acceptor solute, $Cu(acac)_2$, will essentially depend on the charge distribution on the donor atoms. Thus, amines such as pyridine, can provide larger shifts to lower energy in the ligand field transitions, and are characterized by smaller values of the isotropic hyperfine constant, while solvents having functional oxygen donor atoms being of smaller basicity are characterized by larger values of the isotropic hyperfine constant. Overall, these results agree very well with the experimental findings of Adato and Elizer which were obtained in a wide range of different basic solvents.[10]

SUMMARY

The present paper offers theoretical predictions for the solvent effects on the optical and magnetic spectra of Cu(II) acetylacetonate complex by using quantum chemistry methodologies. DFT calculations have been performed using the supermolecule model to describe the direct solvent interactions with the $Cu(acac)_2$ complex. The results indicate that coordination at the axial position of $Cu(acac)_2$ is favored with a high basicity of the solvent. The visible near-infrared absorption transitions as well as the EPR parameters show a strong dependence on the coordination environment around the copper complex. The B3LYP results of the 3d→3d excitation energies show that each model of the solvated model complex gives rise to a particular spectral pattern of the absorption spectrum, where both positions and intensities of electronic transitions can be used to characterize the coordination environment of the first solvation shell around the $Cu(acac)_2$ complex in solution. The good comparison with experimental results indicates that the coordination of the solvent at axial position of $Cu(acac)_2$ should indeed be the main solvent effect on the positions and intensities of absorption bands in $Cu(acac)_2$.

The B38LYP calculations give accurate predictions for the individual components as well as the isotropic values of the **g**-tensors of the $Cu(acac)_2$−pyridine model complexes. On the other hand, the computed results of **A**-tensors show a qualitative agreement with the experimental data available. The deviations from the experimental data are likely caused by the absence of vibrational environmental effects and also due to the fact that the conventional exchange-correlation functionals still remain severely handicapped in their ability to describe EPR parameters of transition metal complexes. The computed excitation energies and EPR parameters give support to the conclusion that the monofold-coordinated $Cu(acac)_2$−solvent system is the most suitable model for describing the optical and magnetic properties of $Cu(acac)_2$ in basic solutions. Compared to the electronic **g**-tensors of the $Cu(acac)_2$ complex, the hyperfine coupling constants show a pronounced dependence on the effect of the base strength of solvent. Overall, the present methodology used in this investigation correctly reproduces the optical and EPR properties of the solvated the $Cu(acac)_2$ models, providing a satisfactory and reliable description of the solvent effects on the optical and magnetic properties of a $Cu(acac)_2$ complex.

REFERENCES

(1) Rorabacher, D. B. *Chem. Rev.* **2004**, *104*, 651.
(2) Orozco, M.; Luque, F. J. *Chem. Rev.* **2000**, *100*, 4187.
(3) N. S. Hush, N. S.; Reimers, J. R. *Chem. Rev.* **2000**, *100*, 775.
(4) Orozco, M.; Luque, F. J. *Chem. Rev.* **2001**, *101*, 203.
(5) Schofield, D. P.; Jordan, K. D. *J. Phys. Chem. A* **2007**, *111*, 7690.
(6) Liu, W. L.; Zheng, Z. R.; Dai, Z. F.; Liu, Z. G.; Zhu, R. B.; Wu, W. Z.; Li, A. H.; Yang, Y. Q.; Su, W. H. *J. Chem. Phys.* **2008**, *128*, 124501.
(7) Huheey, J. E. *Inorganic Chemistry: Principles of Structure an Reactivity*, 3rd ed.; Harper & Row: New York, 1983, Chapter 9.
(8) Ortolano, T. R.; Funck, L. L. *Inorg. Chem.* **1968**, *7*, 537.
(9) Belford, R. L.; Calvin, M.; Belford, G. *J. Chem. Soc. A* **1957**, *26*, 1165.
(10) Adato, I.; Eliezer, I. *J. Chem. Phys.* **1971**, *54*, 1472.
(11) (a) Ames, W. M.; Larsen, S. C. *J. Biol. Inorg. Chem.* **2009**, *14*, 547–557. (b) Ames, W. M.; Larsen, S. C. *Phys. Chem. Chem. Phys.* **2009**, *11*, 8266–8274. (c) Ames, W. M.; Larsen, S. C. *J. Phys. Chem. A* **2010**, *114*, 589–594.
(12) Ames, W. M.; Larsen, S. C. *J. Phys. Chem. A* **2009**, *113*, 4305–4312.
(13) de Almeida, K. J.; Rinkevicius, Z.; Vantras, O.; Ågren, H.; Cesar, A. *Chem. Phys. Lett.* **2010**, *492*, 14–18.
(14) Rinkevicius, Z.; de Almeida, K. J.; Oprea, C. I.; Vahtras, O; Ågren, H.; Ruud, K. *J. Chem. Phys.* **2008**, *129*, 064109.
(15) (a) Neese, F. *Int. J. Quantum Chem.* **2001**, *83*, 104. (b) Neese, F. *J. Chem. Phys.* **2001**, *115*, 11080. (c) Neese, F. *Int. J. Quantum Chem.* **2001**, *83*, 104.
(16) Neese, F. *J. Chem. Phys.* **2003**, *118*, 3939.
(17) Saladino, A. C.; Larsen, S. C. *J. Phys. Chem. A* **2003**, *107*, 5583.
(18) de Almeida, K. J.; Rinkevicius, Z; Ferreira, A. C.; Ågren, H. *Chem. Phys.* **2007**, *332*, 176.
(19) de Almeida, K. J.; Murugan, N. A.; Rinkevicius, Z.; Hugosson, H. W.; Ågren, H.; Cesar, A. *Phys. Chem. Chem. Phys.* **2009**, *11* 508–519.
(20) Schmidt, M. W.; Baldridge, K. K.; Boatz, J. A.; Elbert, S. T.; Gordon, M. S.; Jesen, J. H.; Koseki, S.; Matsunaga, N.; Nguyen, K. A.; Su, S. J.; Windus, T. L.; Dupuis, M.; Montgomery, J. A. *J. Comput. Chem.* **1993**, *14*, 1347–1363.
(21) Rassolov, V.; Pople, J. A.; Ratner, M.; Windus, T. L. *J. Chem. Phys.* **1998**, *109*, 1223–1229.
(22) Krishnan, R.; Binkley, J. S.; Seeger, R.; Pople, J. A. *J. Chem. Phys.* **1980**, *72*, 650–654.
(23) Rinkevicius, Z; Tunell, I.; Sałek, P.; Vahtras, O.; Ågren, H. *J. Chem. Phys.* **2003**, *119*, 34–46.
(24) (a) Becke, A. D. *Phys. Rev. A* **1988**, *38*, 3098–3100. (b) Becke, A. D. *J. Chem. Phys.* **1993**, *98*, 5648–5652.
(25) Lee, C; Yang, W.; Parr, R. G. *Phys. Rev.* **1988**, *37B*, 785–789.
(26) Rinkevicius, Z.; Tunell, I.; Salek, P.; Vahtras, O.; Ågren, H. *J. Chem. Phys.* **2003**, *119*, 34–46.
(27) Solomon, E. I.; Szilagyi, R. K.; DeBeer George, S.; Basumallick, L. *Chem. Rev.* **2004**, *104*, 419–458.

(28) Szilagyi, R. K.; Metz, M.; Solomon, E. I. *J. Phys. Chem. A.* **2002**, *106*, 2994–3007.
(29) Kutzelnigg, W., Fleischer, U., Schindler, M. *In NMR Basic Principles and Progress*; Diehl, P, Fluck, E., Günther, H., Kosfeld, R., Eds.; Springer: Heidelberg, 1990; Vol. 23, pp 165−172.
(30) Huzinaga, S. *Approximate Atomic Functions*; University of Alberta: Edmonton, AB, Canada, 1971; pp 38−39.
(31) Neese, F. *Inorg. Chim. Acta* **2002**, *337C*, 181–192.
(32) Schimmelpfennig, B. *AMFI: An Atomic Spin-Orbit Mean Field Integral Program*; University of Stockholm: Sweden, 1996.
(33) *DALTON, a Molecular Electronic Structure Program*, release 2.0; see http://www.kjemi.uio.no/software/dalton/dalton.html
(34) Thomas, B. G.; Morris, M. L.; Hilderbrant, R. L. *J. Mol. Struct.* **1976**, *35*, 241.
(35) Hitchman, M. A.; Belford, R. L. *Inorg. Chem.* **1971**, *10*, 984–988.
(36) Rinkevicius, Z.; Telyatnyk, L.; Sałek, P.; Vahtras, O.; Ågren, H. *J. Chem. Phys.* **2003**, *119*, 34–46.
(37) Shibata, S.; Sasase, T.; Ohta, M. *J. Mol. Struct.* **1983**, *96*, 889–894.